A 2.45-GHz Rectifier-Booster Regulator With Impedance Matching Converters for Wireless Energy Harvesting

Shiquan Fan, *Member, IEEE*, Zheyi Yuan, Wei Gou, *Student Member, IEEE*, Yang Zhao, Chaoyun Song, *Member, IEEE*, Yi Huang, *Senior Member, IEEE*, Jiafeng Zhou, and Li Geng, *Member, IEEE*

***Abstract*— In this paper, a proof-of-concept high-efficiency rectifier-booster regulator (RBR) with an impedance matching converter operating at 2.45 GHz is proposed. An entire WLAN energy harvesting system is demonstrated. A flower-shaped broadband dual-polarized cross dipole antenna with a full-wave matching network is employed to harvest electromagnetic energy from a WiFi router. A novel RBR is proposed to rectify the RF energy to dc and boost the output voltage. It is evolved from a Greinacher rectifier and two Cockcroft–Walton charge pumps to form a full-wave rectifier. An equivalent resistance model is established to evaluate the optimal stage of the RBR. Furthermore, a boost converter is designed as an impedance matching converter to harvest as much energy as possible from the RBR and store the energy into a 1-mF supercapacitor. Experimental results show that the RBR can provide 1.7-V output voltage under −10-dBm input power. In addition, the RBR can achieve up to ×3.4 voltage boosting with 85% voltage conversion rate (VCR) and provide a higher than 1-V output voltage within a distance of 50 cm between an antenna with 20-dBm transmitting power and the rectenna. The excellent performance shows the wide practicality of the proposed design method for the Internet-of-Things (IoT) applications.**

***Index Terms*— Cockcroft–Walton charge pump, Greinacher rectifier, impedance matching converter, Internet of Things (IoT), rectenna, WLAN energy harvesting.**

I. Introduction

AS THE Internet of Things (IoT) is becoming a hot research field, integrated circuits, which aim at smart home, health care, or environment monitoring applications, have met explosive growth [1]–[3]. In the meantime, the power consumption and energy source of these circuits have attracted wide attention. Ultralow power designs and reliable power sources are necessary for these circuits since many of them are designed to work for tens of years. It is impractical to replace energy source for some specific applications. The concept of harvesting energy from ambient environment has been raised for a long time [4]–[7]. Many types of energy sources such as solar energy and thermal energy have been adopted to power circuits. Nevertheless, the drawbacks restrict the practicability of such sources. For instance, solar energy is very limited at night and thermal energy harvesting breaks down in the environment with a stable temperature. Radio frequency (RF) signals, however, are widely used for mobile communications, radio/TV broadcasting systems, and WiFi networks. RF energy can be harvested anytime and almost anywhere with a rectenna [8]–[13]. The feasibility of RF energy harvesting has been experimentally proved from hardware implementation viewpoint [6], [7], [14]–[17].

Many papers have been published to deal with the problems of RF energy harvesting [2], [3], [18]–[22]. Chen and Chiu [2] focuses on the optimization of antennas to collect more power. Lu *et al.* [3] propose a new rectifier to improve power conversion efficiency (PCE). However, most previous works do not take much consideration on the output voltage features of harvesters. Normally, RF energy is weak and discontinuous, especially under outdoor conditions. Even when the harvester has high energy conversion efficiency, the output voltage is usually very low. Thus, in this case, RF energy cannot be used directly to power the next stage, which usually demands a supply voltage of several V [23]–[24].

In order to guarantee a high-voltage conversion rate (VCR), a simple half-wave rectifier is employed in a 2.45-GHz energy harvesting system [25], but the output voltage of the rectifier is only 0.41 V. Even when a boost converter is cascaded to step up the output voltage to 3.0 V, an additional voltage supply of 1.2 V is needed to enable the normal operation of the boost converter, which is very inconvenience for real applications. A Greinacher rectifier can be used to rectify and boost the output voltage, but the output voltage is still quite low for most ICs [2], [26]–[29]. A conventional Dickson charge pump can be employed as a dc–dc voltage multiplier to further boost the output voltage of the rectifier. However, it suffers from the drawback of high reverse dc bias when

Manuscript received August 1, 2018; revised November 3, 2018 and January 7, 2019; accepted March 14, 2019. This work was supported in part by the National Natural Science Foundation of China under Grant 61504105 and in part by the National Key Research and Development Program of China under Grant 2016YFB0400200. This paper is an expanded version from the IEEE International Wireless Symposium, Chengdu, Sichuan, China, May 6–9, 2018. *(Corresponding authors: Shiquan Fan; Jiafeng Zhou; Li Geng.)*

S. Fan, Z. Yuan, W. Gou, Y. Zhao, and L. Geng are with the School of Electronic and Information Engineering, Xi'an Jiaotong University, Xi'an 710049, China (e-mail: junjunfan@xjtu.edu.cn; gengli@xjtu.edu.cn).

C. Song, Y. Huang, and J. Zhou are with the Department of Electrical Engineering and Electronics, University of Liverpool, Liverpool L69 3GJ, U.K. (e-mail: jiafeng.zhou@liverpool.ac.uk).

Color versions of one or more of the figures in this paper are available online at http://ieeexplore.ieee.org.

Digital Object Identifier 10.1109/TMTT.2019.2910062

TABLE I
COMPARISON OF THE PROPOSED RF ENERGY HARVESTER WITH RECENT REPORTED WORK

	[25] 2018 TMTT	[28] 2016 TMTT	[29] 2018 AWPL	[40] 2013 IMWS	[41] 2013 IMS	**This Work**
Frequency (GHz)	2.45	0.85*, 1.85	2.45*, 5.5	1.8, 2.45*	0.9, 1.8, 2.45*	**2.45**
Rectifier Architecture	Half-wave	Greinacher	Greinacher	Half-wave	Dickson	**RBR**
Number of Stages	1	2	2	1	4	**4**
Peak PCE	56.0%@-10 dBm	44.2%@-10 dBm	36.0%@5 dBm	75.1%**@12 dBm	43%@16 dBm	**37.5%@13 dBm**
Load Resistance @Peak PCE	3 kΩ	9.53 kΩ	12 kΩ	917 Ω	12 kΩ	**20 kΩ**
Output Voltage @-10 dBm	0.41 V***	0.65 V	0.49 V***	0.50 V**	0.24 V***	**1.70 V**
Voltage Improvement	0% (Ref.)	↑ 58%	↑ 20%	↑ 22%	↓ 42%	**↑ 315%**

*: Parameters and results at this frequency;
**: Simulated results;
***: Calculated results through the curves of PCE versus input power and load resistance;

the number of cascading stage increases, which causes low VCR and PCE [30]–[32]. There is still a lack of discussion on the optimal number of stages of the Dickson charge pump to guarantee a high enough output voltage. Also, a Dickson charge pump generates various odd harmonics, which requires complex filters in the circuit [26]. A negative-to-positive voltage converter (NVC) can be used as an active rectifier, which is composed of four MOS transistors connected as a 1-bit static random access memory (SRAM) to realize self-negative driving [5], [33], [34]. However, it can achieve high VCR and PCE only when the voltage from the harvester is around the threshold voltage of the MOS transistors. In order to harvest as much energy as possible, impedance matching design (e.g., boost converter) is also very important for a harvesting system [25], [28], [35]–[37].

At the same time, the dc voltage from a rectifier is more important for some applications, because the poststage circuits (e.g., current bias, bandgap reference, oscillator, or regulator) still need a high voltage (cold startup voltage of active ICs) to maintain their normal operating conditions. Based on the energy harvesting circuit designed in a previous work [27], this paper mainly considers how to boost the output voltage of the rectifier. Table I provides a summary of recent work on RF energy harvesters. Compared with other works, the output voltage of the proposed rectifier is improved significantly at low input power levels. With an input power of −10 dBm, the proposed rectifier can provide 1.70-V output voltage, which is high enough to directly drive most poststage active energy harvesting ICs without any additional voltage source.

Based on the above-mentioned considerations, a proof-of-concept prototype ambient energy harvester is proposed and implemented. The system architecture is shown in Fig. 1. In our previous work, a rectifier-booster regulator (RBR) evolved from a Greinacher rectifier and two Cockcroft–Walton charge pumps were used to form a full-wave rectifier [38]. A complete WLAN energy harvesting system with the maximum power point tracking (MPPT) is introduced in this paper. It includes the design of the rectenna (antenna with RF matching network), the operating principle and modeling of the RBR and the implementation of the impedance matching converter. In our other work [35], a buck-boost converter is adopted as an impedance matching converter to track the maximum power from a piezoelectric cantilever energy source. However, in this work, a boost converter is designed to meet the requirement of the WLAN energy harvesting system. Test results confirm the validity of the proposed analysis and design techniques.

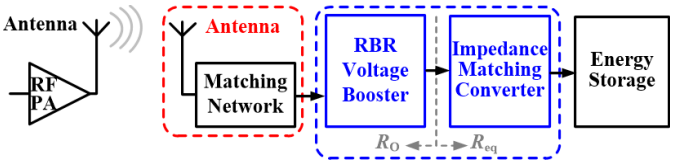

Fig. 1. Architecture of the proposed WLAN energy harvesting system.

This paper is organized as follows. Section II presents the architecture of the proposed WLAN energy harvesting system, which includes the design of the rectenna, the RBR, and the impedance matching converter. Then in Section III, the design consideration is discussed, including the operating principle, the capacitor selection, the equivalent resistance modeling, and the optimal stages of the RBR. Experimental results are given in Section IV. Finally, conclusions are drawn in Section V.

II. ARCHITECTURE OF THE PROPOSED SYSTEM

The architecture and the subblock implementation of the proposed WLAN energy harvesting system are described in this section, including the antenna with an RF matching network, the RBR, and the impedance matching converter.

A. Architecture of the System

The architecture of the proposed WLAN energy harvesting system is shown in Fig. 1. It includes an RF power amplifier (PA) with an antenna (WiFi Router), a receiving antenna with matching network, an RBR voltage booster, an impedance matching converter, and an energy storage unit (super capacitor or rechargeable battery). Electromagnetic energy radiated from the antenna is harvested by a dual-polarized cross dipole antenna with an RF matching network. A novel RBR is

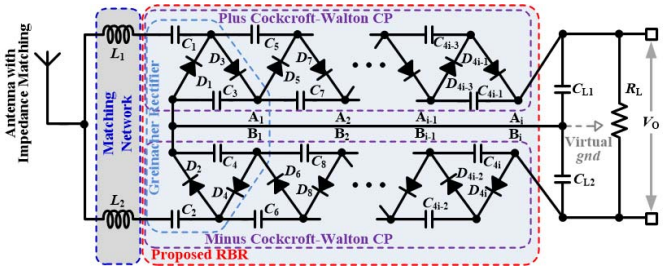

Fig. 2. Circuit implementation of the proposed RBR.

proposed to rectify RF power to dc and boost the output voltage. Then, a dc–dc converter with dc impedance matching is employed to maximize the harvested energy.

B. Rectenna Design

With the diffusion of signal from an RF source, its power density will decrease fast with distance. This makes wireless energy harvesting difficult over a long distance, especially when using an omnidirectional antenna as the source. The power captured, P_{RX}, by an omnidirectional antenna is

$$P_{\mathrm{RX}} = \left(P_{\mathrm{TX}} \times \frac{1}{4\pi R^2}\right) \times \left(\frac{\lambda^2 G}{4\pi}\right) \tag{1}$$

where the former part of (1) is the density of the transmit power P_{TX} in free space with a distance of R, the latter is the effective area of the receiving antenna, λ is the wavelength of the carrier, and G is the antenna gain. P_{TX} of a normal source, typically a WiFi router, is usually limited to 20-dBm. With a 20-dBm omnidirectional source, the power density in free space can be calculated. Since the power density reduces quite rapidly with R, a rectenna has to be carefully designed to improve the level of harvested power.

A flower-shaped broadband dual-polarized cross dipole antenna with an RF matching network [27] is employed to harvest electromagnetic energy from a WiFi router. The electromagnetic energy is transformed into RF energy. The cross dipole antenna is selected due to its planar shape and dual polarization, which is suitable for incoming signals with arbitrary polarizations. A flower-shaped slot filter is designed on the patch antenna to suppress harmonics. A matching network is devised and optimized for a good match with a wide range of input power. The antenna has a gain of 3.9 dB and a return loss of better than −12 dB at 2.45 GHz.

This rectenna can achieve high efficiency over a very wide band. It can also potentially harvest energy from other resources, such as mobile communication signals. A two-branch matching network with a full-wave rectifier is used so that high performance can be achieved even with a relatively low power density. The rectenna has a maximum conversion efficiency of around 55% for −10-dBm input power. Considering the high dc power output of this design in a relatively low power density environment, this rectenna can be used for efficient wireless energy harvesting for a wide range of the wireless sensor and network applications.

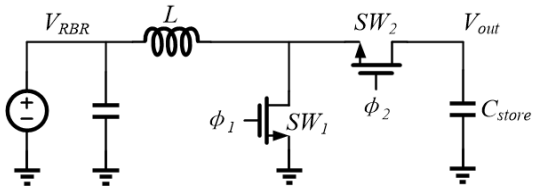

Fig. 3. Power stages of the boost converter for impedance matching.

C. RBR implementation

Normally, a Greinacher rectifier, formed by $C_{1\sim4}$ and $D_{1\sim4}$ as shown in Fig. 2, works as a voltage quadrupler. During the positive cycle of an RF signal, C_2 is charged to V_N through the C_2–D_2path. During the negative cycle, C_1 is charged to V_P through the C_1–D_1 path. Meanwhile, C_4 is charged to $2V_N$ through the C_4–D_4–C_2 path. During the next positive cycle, C_3 is charged to $2V_P$ through the C_1–D_3–C_3 path. Thus, totally twice the differential voltage between nodes A_1 and B_1 can be obtained with four diodes and four capacitors.

A Greinacher rectifier can be divided into two separate two-stage Cockcroft–Walton charge pumps connected to virtual ground (gnd). Even though a Greinacher rectifier can boost the output voltage of a rectenna, the voltage may still be too low to power the next stage directly, especially when the RF signal is weak. If more boosting stages are cascaded after nodes A_1 and B_1, the output voltage can be further increased.

Therefore, an RBR is proposed in this paper, where A_i and B_i are the output nodes of the ith-stage RBR, as shown in Fig. 2. It is evolved from a Greinacher rectifier and a Cockcroft–Walton charge pump to rectify RF energy received by the antenna to dc and to simultaneously boost the output voltage. The RBR combines the merits of both the Greinacher rectifier and the Cockcroft–Walton charge pump. Here, the Cockcroft–Walton charge pump is not simply connected after the Greinacher rectifier. The Greinacher rectifier not only functions as a rectifier but also forms the initial stages of the Cockcroft–Walton charge pump.

D. Impedance Matching Converter

The function of the impedance matching converter is to realize a constant input impedance R, which should be equal to the output impedance R_o of the RBR [37], [39]. When $R_{\mathrm{eq}} = R_o$, the maximum power can be harvested, as shown in Fig. 1.

Since the output of the previous stages is nearly constant, a dc source with a steady voltage V_{RBR} is used to represent the antenna and RBR. The impedance matching converter is then built with control signals φ_1 and φ_2, as shown in Fig. 3. The waveform of the inductor current in one switching period is shown in Fig. 4. The pulse frequency modulation (PFM) control method is applied. φ_1 as the PFM signal is active for a constant time, which determines t_{on} as shown in Fig. 4. φ_2 is used to release the energy stored in the inductor. For the boost converter operating in an asynchronous mode, SW_2 can be replaced by a diode. Thus, φ_2 is no longer needed. T is the switching period of the PFM signal.

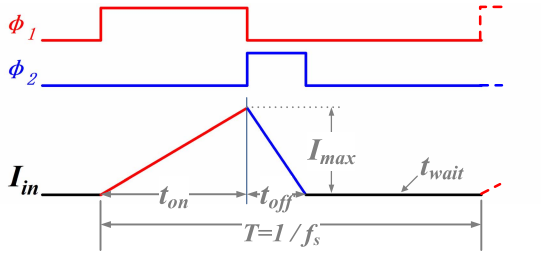

Fig. 4. Waveform variation of the inductor current in one switching period.

During the charging time t_{on}, the voltage difference between V_{RBR} and gnd builds up current in the inductor. The relationship between the current and the voltage of the inductor can be described by

$$u_{\text{ind}} = L\frac{di_{\text{ind}}}{dt} \tag{2}$$

$$i_{\text{ind}} \equiv i_{\text{in}} = \int_0^{t_{\text{on}}} \frac{u_{\text{ind}}}{L} dt. \tag{3}$$

Since $u_{\text{ind}} = V_{\text{RBR}}$ during the charging time, the expression of the inductor current can be rewritten as

$$I_{\text{in}} = \frac{V_{\text{RBR}}}{L}t, \quad t \in [0, t_{\text{on}}] \tag{4}$$

$$I_{\text{max}} = \frac{V_{\text{RBR}}}{L}t_{\text{on}}. \tag{5}$$

During the discharging period t_{off}, the inductor is connected to C_{store}. The inductor current begins to decrease with a higher V_{out}. It can be obtained

$$t_{\text{off}} = \frac{V_{\text{RBR}}}{V_{\text{out}} - V_{\text{RBR}}}t_{\text{on}}. \tag{6}$$

Then, the power of the boost converter can be calculated and its average power is used to calculate the equivalent resistance. The energy from the RBR during each cycle can be expressed by

$$E = (t_{\text{on}} + t_{\text{off}}) \cdot V_{\text{RBR}} \cdot I_{\text{avg}} \tag{7}$$

where I_{avg} is the average inductor current in the period of t_{on} and t_{off}, which is equal to $I_{\text{max}}/2$. E is related to both t_{on} and t_{off}. However, t_{off} can be much smaller than t_{on} for high VCR, thus (7) can be approximated to

$$E \approx t_{\text{on}} \cdot V_{\text{RBR}} \cdot \frac{I_{\text{max}}}{2} = \frac{V_{\text{RBR}}^2 \cdot t_{\text{on}}^2}{2L}. \tag{8}$$

Finally, the average power and the equivalent resistance are

$$P_{\text{avg}} = \frac{E}{T} = \frac{V_{\text{RBR}}^2 \cdot t_{\text{on}}^2}{2L} f_{\text{PFM}} \tag{9}$$

$$R_{\text{eq}} = \frac{V_{\text{RBR}}^2}{P_{\text{avg}}} = \frac{2L}{t_{\text{on}}^2 \cdot f_{\text{PFM}}}. \tag{10}$$

For a specific L of 820 μH, the relationship between R_{eq} and the maximum PFM switching frequency f_{PFM} of the boost converter under different t_{on} time is shown in Fig. 5. It can be seen that with the increase in t_{on}, the input energy of the boost converter in one switching period will increase, determined by (8). In order to keep R_{eq} constant to match R_o of the RBR, the required f_{PFM} will decrease significantly.

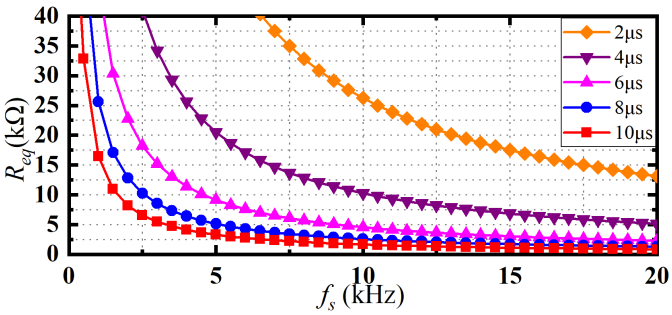

Fig. 5. Calculated R_{eq} versus f_{PFM} under different t_{on}.

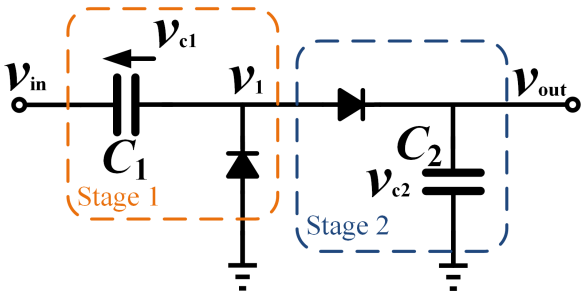

Fig. 6. Stage division of a Greinacher rectifier.

III. Design Considerations

To further analyze the features of the RBR, the detailed design consideration including circuit modeling and discussion are presented in the following sections.

A. Modeling of the RBR

It is a challenging task to analyze the whole structure altogether. To make it easier, the RBR structure is divided into discrete stages. Each stage consists of one capacitor and one diode on each half side of a full-wave regulator. It means that a Greinacher rectifier is split into two stages. Usually, the startup time of a rectifier is much longer than the cycle length of a signal. In the analysis, a fast model is considered where a steady state can be reached in one cycle.

The stage division is shown in Fig. 6. Stage 1 is used to shift the dc level of the signal, whereas Stage 2 can hold the output voltage at the peak value. The startup waveforms of each single stage and the combination of them are shown in Fig. 7. The input signal, v_{in}, is assumed to be a sine wave with an amplitude of V_{amp}. In Stage 1, v_1 follows v_{in} in the positive half-cycle. In the negative half-cycle, v_1 is connected to ground by the diode, and the capacitor C_1 can be charged to its maximum voltage V_{amp}. Therefore, the output of Stage 1, v_1, in the steady state is

$$v_1 = v_{\text{in}} + V_{\text{amp}}. \tag{11}$$

In Stage 2, the diode allows C_2 to be charged by $v_{\text{in},2}$ in the positive half-cycle and makes it not dischargeable from this path. Therefore, C_2 will hold the peak value of $v_{\text{in},2}$. The output of Stage 2 (v_2) in the steady state is

$$v_2 = \max(v_{\text{in},2}). \tag{12}$$

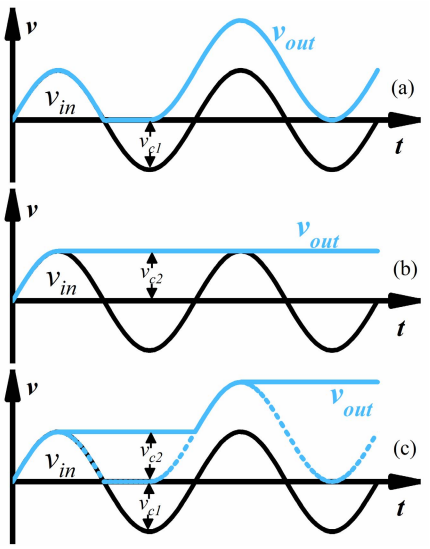

Fig. 7. Startup waveforms of (a) stage 1, (b) stage 2, and (c) both stages.

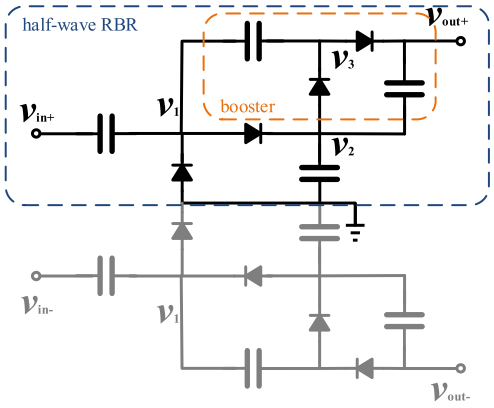

Fig. 8. Full-wave rectifier cascaded by one booster stage.

Thus, the output of a Greinacher rectifier in the steady state can be expressed as

$$v_{\text{out}} = \max(v_{\text{in}} + V_{\text{amp}}) = 2V_{\text{amp}}. \tag{13}$$

In order to further increase the output voltage level, more stages can be cascaded after the rectifier as boost stages. In Fig. 8, a booster is connected to the rectifier by using v_1 as the input and v_2 as the virtual ground.

The operation of the additional booster is similar to the first stage. However, it should be noted that v_2 is higher than v_1. The maximum voltage difference between them is about $2V_{\text{amp}}$. Therefore, the booster can increase the output voltage by $2V_{\text{amp}}$. To implement a full-wave regulator, another half-wave RBR is built and connected in the opposite direction, as shown in the grey part of Fig. 8.

The output of a full-wave RBR can be given by

$$v_{\text{out}} = v_{\text{out}+} - v_{\text{out}-} = 4V_{\text{amp}} - (-4V_{\text{amp}}) = 8V_{\text{amp}}. \tag{14}$$

The output of an RBR with N-stage rectifiers or boosters should be

$$v_{\text{out},N} = 4NV_{\text{amp}}. \tag{15}$$

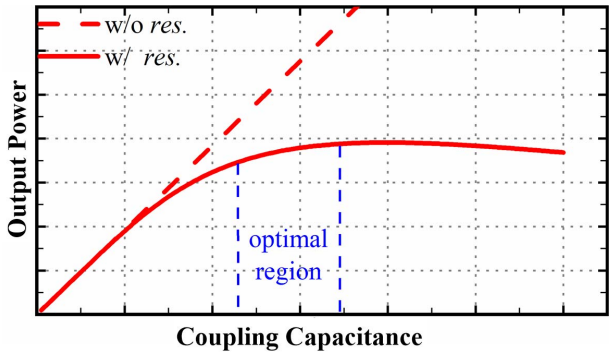

Fig. 9. Relationship between the coupling capacitance and the output power.

B. Capacitor Selection of the RBR

For a charge pump operating at a constant frequency, a small value of the flying capacitance means low output power. However, a large value could not always ensure high output power either. There is an optimal range that is mainly determined by the parasitic resistance of the connecting wire, switches, and the operating frequency of the charge pump.

To maximize the output voltage and the power of the proposed regulator, an optimal choice of component values is necessary. In the ideal case, energy can be fully transferred and stored into capacitors if the parasitic resistance of all components is negligible. However, it is no longer the case after the parasitic resistance is considered.

In each cycle, the coupling capacitor C_1 is first charged during the negative half-cycle, and then the energy is transferred into the storage capacitor C_2. The steady state is considered here to help build the model.

The power available from a capacitor can be given by

$$P = \frac{1}{2}CV^2 f. \tag{16}$$

The voltage on the capacitor during each charge cycle can be expressed by

$$V = V_c\left(1 - e^{-\frac{t}{RC}}\right) \tag{17}$$

where V_c is the equivalent charge voltage, f is the operating frequency of the charge pump, and t is the charging time in each cycle. These are considered to be constant in the steady state. C is the coupling capacitor and R is the serial parasitic resistor that is mainly from the diode. Therefore, with a specific resistance (SMS7630 in our case), the optimal range of capacitance can be shown in Fig. 9 by combining (16) and (17). The selection of the center point is based on the extreme low point of the second derivative. An optimal value of the coupling capacitance can be chosen to achieve the highest output power.

C. Equivalent Resistance of the RBR

In the ideal case, the output voltage can be increased by further cascading boosters without limitation. Even when the voltage drop on diodes is taken into consideration, this tendency will only slow down. However, this is not

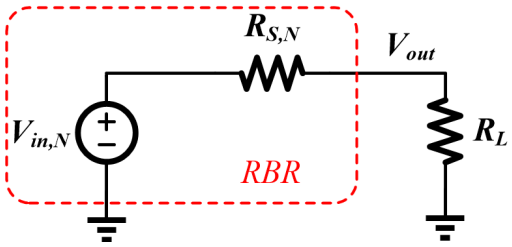

Fig. 10. Equivalent resistance model of the RBR.

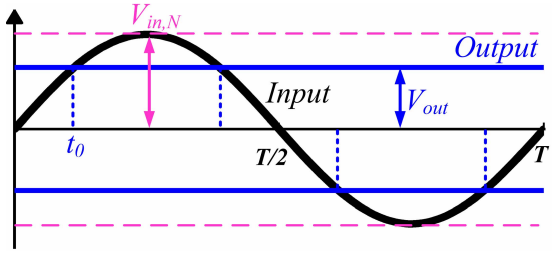

Fig. 11. Waveforms illustration of the input and output voltages of the equivalent resistance model of the RBR shown in Fig. 10.

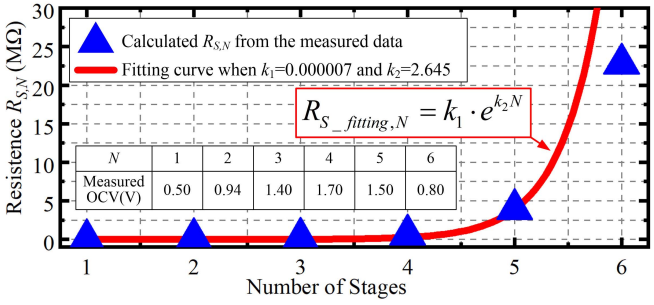

Fig. 12. Calculated data and curve fitting of $R_{S,N}$ versus number of stages.

practical due to that only limited power can be harvested by the rectenna.

When the input power is sufficient, each node in the RBR can be charged to the maximum value. However, in real conditions, the input power is usually limited, and the load effect cannot be neglected. When the harvesting power is not enough to drive the load at all stages, the output voltage will go down, and it will also limit the total output power. Therefore, the feature of the internal equivalent resistance of the RBR needs to be studied.

Here, an equivalent resistance model of the RBR is shown in Fig. 10. R_L is the load resistance, which is 10 MΩ of the probe in this case. $R_{S,N}$ is the internal equivalent resistance of the N-stage RBR. $V_{\text{in},N}$ is the ideal output voltage of the N-stage RBR given in (15), which satisfies

$$V_{\text{in},N} = V_{\text{out},N} = 4NV_{\text{amp}}. \tag{18}$$

According to Fig. 10, if $R_{S,N}$ is much smaller than R_L, the output voltage, V_{out}, can be close to the ideal case. That is, $V_{\text{out}} = V_{\text{in},N}$. If $R_{S,N}$ is comparable to or larger than R_L, the voltage drop on $R_{S,N}$ cannot be ignored, which causes a decrease in V_{out}. In order to carefully study the feature of $R_{S,N}$, the input and output voltage waveforms of the equivalent resistance model of the RBR are illustrated in Fig. 11.

The energy consumed at R_L in a period T can be calculated by

$$E_L = P_L \cdot T = \frac{V_{\text{out}}^2}{R_L} \cdot T \tag{19}$$

where V_{out} and R_L represent the output voltage and the load resistance shown in Fig. 10, respectively.

On the other hand, the energy provided by the RBR can be expressed as

$$E_{\text{in}} = \overline{I_{\text{in}}} \cdot V_{\text{out}} \cdot t_\theta \tag{20}$$

where $\overline{I_{\text{in}}}$ is the average current within t_θ. t_θ is the conduction period, which satisfies

$$\begin{cases} t_\theta = T - 4t_0 \\ t_0 = \dfrac{T}{2\pi} \arcsin\left(\dfrac{V_{\text{out}}}{V_{in,N}}\right) \end{cases} \tag{21}$$

where T is the period of the sine wave, and t_0 is the moment when the input voltage becomes larger than the output voltage.

Because $E_L = E_{\text{in}}$, the average current and $R_{S,N}$ can be obtained by

$$\overline{I_{\text{in}}} = \frac{V_{\text{out}}}{R_L} \cdot \frac{T}{T - 4t_0} = \frac{V_{\text{out}}}{R_L\left(1 - 4\frac{t_0}{T}\right)} \tag{22}$$

$$R_{S,N} = \frac{V_{\text{in},N} - V_{\text{out}}}{\overline{I_{\text{in}}}} = \left(\frac{V_{\text{in},N}}{V_{\text{out}}} - 1\right)\left(1 - \frac{2}{\pi}\arcsin\left(\frac{V_{\text{out}}}{V_{\text{in},N}}\right)\right) R_L. \tag{23}$$

Based on (23), $R_{S,N}$ can be easily calculated in various stages by using the measured V_{out}, which is the output voltage under a certain value of R_L of the RBR. Here, the measured open circuit voltage (OCV) under 10 MΩ R_L of the probe is used to calculate the real equivalent $R_{S,N}$ as shown in Fig. 12.

It can be seen that $R_{S,N}$ has a small value when the number of stages is less than 4, and $R_{S,N}$ increases when the number of stages is increased to 5 and 6. This results in a turning point of the output voltage between the fourth- and fifth-stage cases. The reason is that with fewer stages, the power harvested by the rectenna is sufficient to operate the RBR and the load. Thus, the output voltage is close to the ideal value. With more stages, the required power increases quadratically, which may exceed the supply capacity of the rectenna. A high number of stages leads to the rapid increase in $R_{S,N}$. Eventually, the output voltage begins to decrease.

Considering the variation tendency of the calculated $R_{S,N}$, exponential fitting is preferred to describe $R_{S,N}$. The fitting formula can be expressed as

$$R_{S\_\text{fitting},N} = k_1 \cdot e^{k_2 N} \tag{24}$$

where k_1 and k_2 are the coefficients that can be obtained by using only two values of $R_{S,N}$. Here, the measured OCVs of Stages 1 and 5 are used to calculate $R_{S,1}$ and $R_{S,5}$.

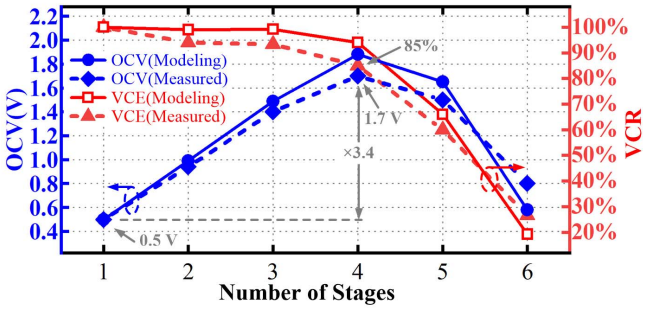

Fig. 13. Comparison of the calculated (from the models) and measured OCV and VCR versus the number of stages.

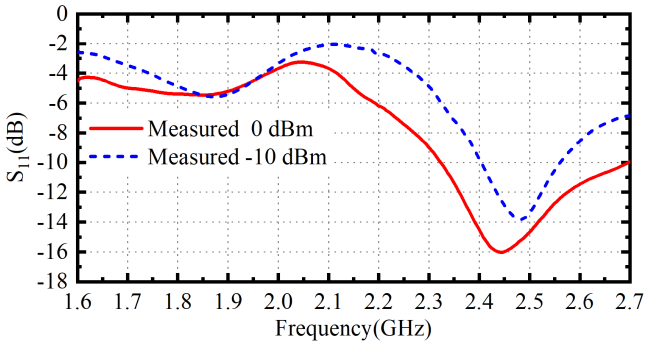

Fig. 14. Measured S_{11} of the RBR with the matching network.

The coefficients of k_1 and k_2 can be solved as 0.000007 and 2.645, respectively. The fitted curve is also plotted in Fig. 12. It shows very good agreement with the calculated one.

D. Number of Booster Stages

According to the above analysis, k_1 and k_2 can be calculated by using only two sets of the measured data, thus the output voltage can be extracted from (23). This process makes it possible to accurately predict the variation tendency and improvement effect of the output voltage by only using very limited data.

In order to verify the accuracy of the equivalent resistance model, the output voltage of the RBR is analyzed. Here, the VCR is used and defined by $V_{\text{out}}/V_{\text{in},N}$. The output voltage of the first stage is considered to be equal to the ideal output. Then, the ideal output voltage of the Nth-stage should be N times of that of the first stage. The calculated and measured OCV and VCR are shown in Fig. 13. Here, it is difficult to exactly solve V_{out} from (23) directly. The measured and modeling results have some disagreement. The data points shown in Fig. 13 do not perfectly match each other. It can be seen that the OCV increases rapidly before the turning point, and decreases dramatically after this point. The measured results match the modeling ones very well. The average error is less than 10%, which verifies the correctness of the model and the relevant theoretical analysis.

IV. Experimental Results

A. RBR Measurement

The performance of the proposed RBR with the matching network is measured at different RF input power levels as shown in Fig. 14. The measured reflection coefficient S_{11} of the RBR is better than -10 dB between 2.4 and 2.5 GHz when the input power to the RBR is in the range of interest, i.e., from -10 to 0 dBm.

The RF-to-dc PCE can be expressed as

$$\eta = \frac{P_{\text{out}}}{P_{\text{in}}} = \frac{V_{\text{out}} \cdot I_{\text{out}}}{P_{\text{in}}} = \frac{V_{\text{out}}^2}{R_L \cdot P_{\text{in}}} \tag{25}$$

where P_{in} is the input power from the RF source and P_{out} is the dc output power that can be obtained by measuring the output voltage on the load R_L.

An RF signal generator (RIGOL DSG3060) is used as the input RF source. The measured output voltage versus input power is shown in Fig. 15(a). Since the output voltage and efficiency are highly dependent on the load resistance, the measurements were carried out with R_L = 500 Ω, 2 kΩ, 10 kΩ, 20 kΩ, 30 kΩ, 65 kΩ, and 10 MΩ (Probe), respectively. For safe operation, each measurement is stopped when the output voltage reaches 14 V. The proposed RBR can provide a 5.9-V output voltage under 0-dBm input power or larger than 1 V under −14-dBm input power with 10-MΩ load resistance. The measured RF-to-dc PCE versus input power is shown in Fig. 15(b). The peak PCE of 37.5% is achieved with 13-dBm input power and 20-kΩ load resistance.

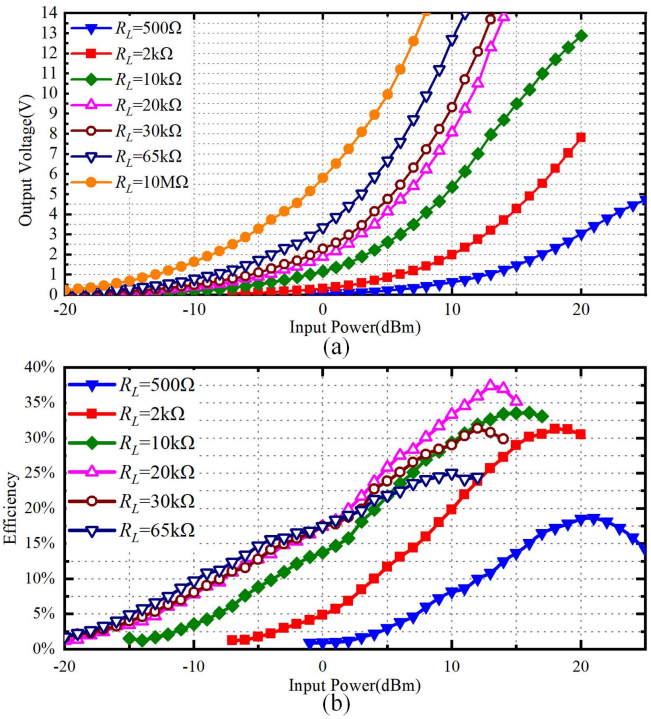

Fig. 15. Measured (a) output voltage and (b) PCE of the RBR versus RF input power with various load impedances.

B. Wireless Experiment

The test platform of the proposed full system is shown in Fig. 16. A four-stage RBR was adopted for the experiment. The RF signal is generated by a signal generator. A PA with 11-dB gain is used to magnify the RF signal. The input

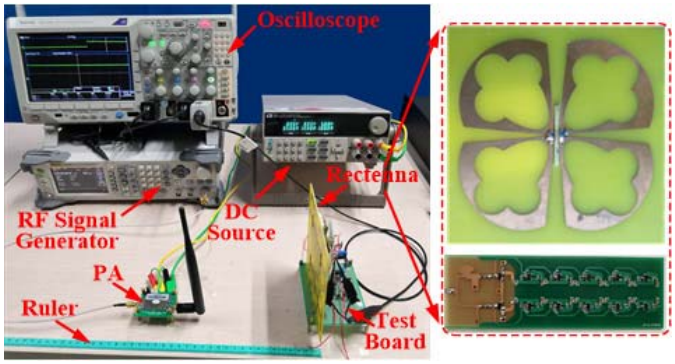

Fig. 16. Test platform of the proposed RF energy harvester.

TABLE II
PARAMETERS OF THE WLAN ENERGY HARVESTING SYSTEM

System Architecture	Rectenna+RBR+Boost Converter	
RBR	RF Frequency	2.45 GHz
	Stages	4
	Flying Capacitor	100nF×16
	Diode	SMS7630×8
	Output Capacitor	10 μF
Boost Converter	Inductor	820 μH
	Switch	2N7002
	Diode	SMS7630
	Output Capacitor	1 mF
	Max. PFM Frequency	10 kHz
	Constant turn-on time	2.5 μs

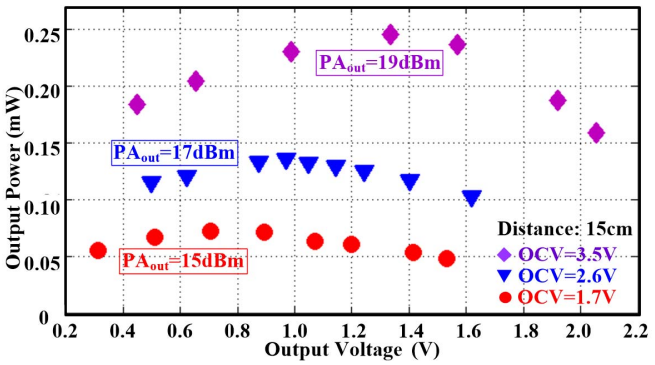

Fig. 17. Measured output power versus output voltage under different load impedances at three different output power levels of the PA.

power of the harvester from the rectenna can be changed by varying the magnitude of the RF signal or the distance between the antenna and the harvester. Parameters of the developed WLAN energy harvesting system are given in Table II. The input impedance of the boost converter can be calculated by employing (10), which should match the output impedance of the RBR.

Since the proposed harvester focuses on indoor RF energy harvesting, 2.45-GHz signals are commonplace in such environment (WiFi networks, ZigBee, or Bluetooth communications) and are employed for the system test in this paper. Fig. 17 shows the measured results of the output power versus output voltage of the proposed system under different load impedances at three different power levels of the RF signal.

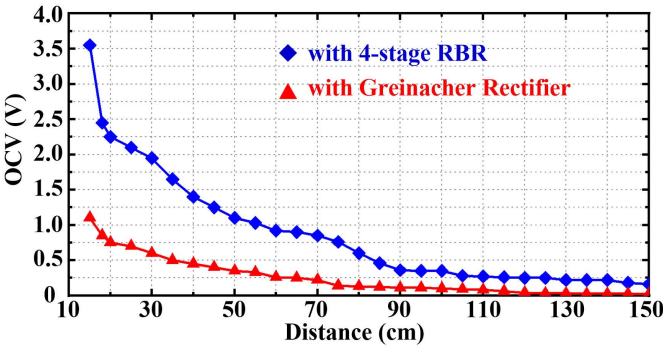

Fig. 18. Measured OCV of the proposed system and the Greinacher rectifier versus the distance between the antenna and rectenna.

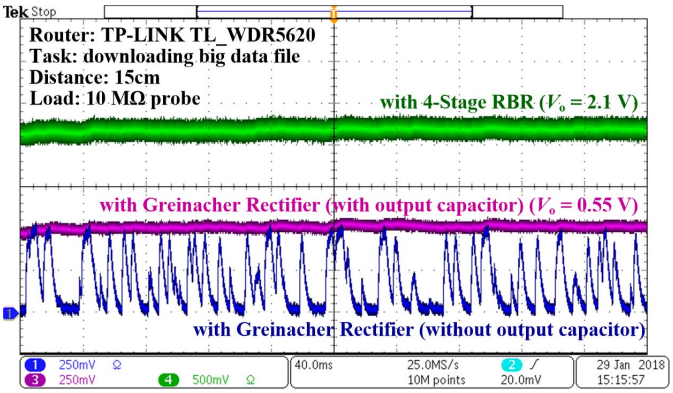

Fig. 19. Measured output voltage when harvesting WLAN energy from a WiFi router.

The distance between the antenna and the rectenna is set to 15 cm, and the magnitude of the RF signal is varied. When the output powers of the PA are 15, 17, and 19 dBm, and the measured OCVs are 1.7, 2.6, and 3.5 V, respectively. Keeping the output power of the PA at 19 dBm, when the distance is increased to 25, 40, and 50 cm, the measured OCVs are 2.1, 1.3, and 1.0 V, respectively. Compared with [2]–[4], the proposed harvester boosts the output voltage to higher levels. This is very desirable for many IoT applications. Also as shown in Fig. 17, all three scatter curves of the output power exhibit a single peak characteristic, which indicates the possibility of applying the MPPT technique to further improve the performance of the harvester.

Normally, the output power of a WiFi router is no more than 20 dBm. In this experiment, a PA is employed to simulate the operation of a WiFi router as an energy source. To facilitate comparison of our design, both a Greinacher rectifier and a four-stage RBR voltage booster are implemented. Fig. 18 shows the measured results of the OCV versus the distance between the transmit antenna and the rectenna. It indicates that the proposed system can provide over 1- and 0.5-V output voltages within a distance of 50 and 90 cm, respectively. Compared with the Greinacher rectifier, the proposed system can boost the output voltage up to 3.4 times higher. The distance can be increased further by using a higher gain antenna.

The proposed system is used to harvest energy from a WiFi router (TP-LINK TL_WDR5620) with a distance of 15 cm

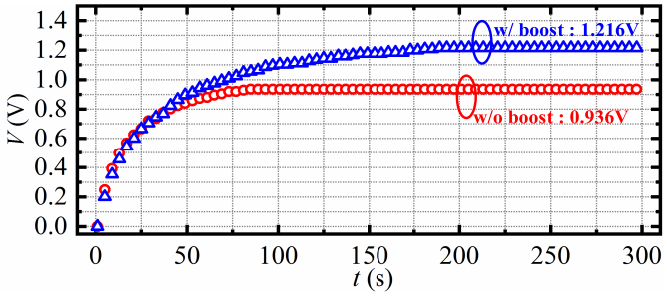

Fig. 20. Measured charging process of a 1-mF capacitor with and without the boost converter.

while the router is downloading a big data file. Fig. 19 shows the transient waveforms of the output voltage of the harvester with a Greinacher rectifier (with and without an output capacitor) and with the four-stage RBR. It can be seen that the harvester with the RBR increases the output voltage significantly. Such measured results have further demonstrated the feasibility of harvesting WLAN energy by using the proposed RF energy harvesting system.

To optimize the available power of the RBR, the charging process of a 1-mF supercapacitor is measured. A boost converter is employed to match the impedance and maximize the harvested power. A PFM frequency of 10 kHz and turn-on time of 2.5 μs are used to realize the input impedance of 20 kΩ of the boost converter to match the output impedance of the RBR. The charging process is shown in Fig. 20. The steady output voltages with and without the boost converter under 10-MΩ load resistance are 1.216 and 0.936 V, respectively. The output power can be calculated by using the equation of $P = V^2/R$, which shows that the output power is increased by nearly 70% after using an impedance matching converter.

V. Conclusion

To sum up, a novel high VCR RBR with an impedance matching converter has been proposed to harvest wireless energy from the WLAN. The RBR is evolved from a Greinacher rectifier and a Cockcroft–Walton charge pump to form a full-wave rectifier. An equivalent resistance model of the RBR is established to accurately predict the variation tendency of the output voltage by only using very limited data. The measured results show that nearly 315% output voltage improvement is achieved with the RBR. Then, combined with a flower-shaped broadband dual-polarized cross-dipole antenna and a boost converter as an impedance matching converter, the entire WLAN energy harvesting system is demonstrated. It harvests RF energy from a WiFi router and stores the electric energy in a supercapacitor. Compared with directly charging a supercapacitor by the RBR, nearly 70% more energy has been harvested by adding an impedance matching converter between the RBR and the supercapacitor. These merits prove the excellent practicality of the proposed harvesting system for IoT applications.

Acknowledgment

The authors would like to thank Dr. M. Ye of XJTU for the helpful technical discussions.

References

[1] T. Wu and H. C. Yang, "RF energy harvesting with cooperative beam selection for wireless sensors," *IEEE Wireless Commun. Lett.*, vol. 3, no. 6, pp. 585–588, Dec. 2014.

[2] Y.-S. Chen and C.-W. Chiu, "Maximum achievable power conversion efficiency obtained through an optimized rectenna structure for RF energy harvesting," *IEEE Trans. Antennas Propag.*, vol. 65, no. 5, pp. 2305–2317, May 2017.

[3] Y. Lu *et al.*, "A wide input range dual-path CMOS rectifier for RF energy harvesting," *IEEE Trans. Circuits Syst. II, Express Briefs*, vol. 64, no. 2, pp. 166–170, Feb. 2017.

[4] U. Olgun, C.-C. Chen, and J. L. Volakis, "Investigation of rectenna array configurations for enhanced RF power harvesting," *IEEE Antennas Wireless Propag. Lett.*, vol. 10, pp. 262–265, Apr. 2011.

[5] K. R. Sadagopan, J. Kang, Y. Ramadass, and A. Natarajan, "A 960pW co-integrated-antenna wireless energy harvester for WiFi backchannel wireless powering," in *IEEE Int. Solid-State Circuits Conf. (ISSCC) Dig. Tech. Papers*, San Francisco, CA, USA, Feb. 2018, pp. 136–138.

[6] E. Falkenstein, M. Roberg, and Z. Popovic, "Low-power wireless power delivery," *IEEE Trans. Microw. Theory Techn.*, vol. 60, no. 7, pp. 2277–2286, Jul. 2012.

[7] Y. Han, O. Leitermann, D. A. Jackson, J. M. Rivas, and D. J. Perreault, "Resistance compression networks for radio-frequency power conversion," *IEEE Trans. Power Electron.*, vol. 22, no. 1, pp. 41–53, Jan. 2007.

[8] Y.-J. Ren and K. Chang, "5.8-GHz circularly polarized dual-diode rectenna and rectenna array for microwave power transmission," *IEEE Trans. Microw. Theory Techn.*, vol. 54, no. 4, pp. 1495–1502, Jun. 2006.

[9] Z. Harouni, L. Cirio, L. Osman, A. Gharsallah, and O. Picon, "A dual circularly polarized 2.45-GHz rectenna for wireless power transmission," *IEEE Antennas Wireless Propag. Lett.*, vol. 10, pp. 306–309, Apr. 2011.

[10] H. Sun, Y.-X. Guo, M. He, and Z. Zhong, "A dual-band rectenna using broadband Yagi antenna array for ambient RF power harvesting," *IEEE Antennas Wireless Propag. Lett.*, vol. 12, pp. 918–921, Jul. 2013.

[11] M. Stoopman, S. Keyrouz, H. J. Visser, K. Philips, and W. A. Serdijn, "Co-Design of a CMOS rectifier and small loop antenna for highly sensitive RF energy harvesters," *IEEE J. Solid-State Circuits*, vol. 49, no. 3, pp. 622–634, Mar. 2014.

[12] M. A. Abouzied and E. Sánchez-Sinencio, "Low-input power-level CMOS RF energy-harvesting front end," *IEEE Trans. Microw. Theory Techn.*, vol. 63, no. 11, pp. 3794–3805, Nov. 2015.

[13] J. Bito, J. G. Hester, and M. M. Tentzeris, "Ambient RF energy harvesting from a two-way talk radio for flexible wearable wireless sensor devices utilizing inkjet printing technologies," *IEEE Trans. Microw. Theory Techn.*, vol. 63, no. 12, pp. 4533–4543, Dec. 2015.

[14] M. PiÃ±uela, P. D. Mitcheson, and S. Lucyszyn, "Ambient RF energy harvesting in urban and semi-urban environments," *IEEE Trans. Microw. Theory Techn.*, vol. 61, no. 7, pp. 2715–2726, Jul. 2013.

[15] J.-P. Curty, N. Joehl, F. Krummenacher, C. Dehollain, and M. J. Declercq, "A model for μ-power rectifier analysis and design," *IEEE Trans. Circuits Syst. I, Reg. Papers*, vol. 52, no. 12, pp. 2771–2779, Dec. 2005.

[16] V. Kuhn, C. Lahuec, F. Seguin, and C. Person, "A multi-band stacked RF energy harvester with RF-to-DC efficiency up to 84%," *IEEE Trans. Microw. Theory Techn.*, vol. 63, no. 5, pp. 1768–1778, May 2015.

[17] M. A. Abouzied, K. Ravichandran, and E. Sánchez-Sinencio, "A fully integrated reconfigurable self-startup RF energy-harvesting system with storage capability," *IEEE J. Solid-State Circuits*, vol. 52, no. 3, pp. 704–719, Mar. 2017.

[18] A. K. Moghaddam, J. H. Chuah, H. Ramiah, J. Ahmadian, P. I. Mak, and R. P. Martins, "A 73.9%-efficiency CMOS rectifier using a lower DC feeding (LDCF) self-body-biasing technique for far-field RF energy-harvesting systems," *IEEE Trans. Circuits Syst. I, Reg. Papers*, vol. 64, no. 4, pp. 992–1002, Apr. 2017.

[19] T.-H. Lin, J. Bito, J. G. Hester, J. Kimionis, R. A. Bahr, and M. M. Tentzeris, "Ambient energy harvesting from two-way talk radio for on-body autonomous wireless sensing network using inkjet and 3D printing," in *IEEE MTT-S Int. Microw. Symp. Dig.*, Honolulu, HI, USA, Jun. 2017, pp. 1034–1037.

[20] G. Papotto, F. Carrara, and G. Palmisano, "A 90-nm CMOS threshold-compensated RF energy harvester," *IEEE J. Solid-State Circuits*, vol. 46, no. 9, pp. 1985–1997, Sep. 2011.

[21] J. Masuch, M. Delgado-Restituto, D. Milosevic, and P. Baltus, "Co-integration of an RF energy harvester into a 2.4 GHz transceiver," *IEEE J. Solid-State Circuits*, vol. 48, no. 7, pp. 1565–1574, Jul. 2013.
[22] Z. Popović *et al.*, "Scalable RF energy harvesting," *IEEE Trans. Microw. Theory Techn.*, vol. 62, no. 4, pp. 1046–1056, Apr. 2014.
[23] T. Sakamoto, Y. Ushijima, E. Nishiyama, M. Aikawa, and I. Toyoda, "5.8-GHz series/parallel connected rectenna array using expandable differential rectenna units," *IEEE Trans. Antennas Propag.*, vol. 61, no. 9, pp. 4872–4875, Sep. 2013.
[24] S.-T. Khang, D.-J. Lee, I.-J. Hwang, T.-D. Yeo, and J.-W. Yu, "Microwave power transfer with optimal number of rectenna arrays for midrange applications," *IEEE Antennas Wireless Propag. Lett.*, vol. 17, no. 1, pp. 155–159, Jan. 2018.
[25] S.-E. Adami *et al.*, "A flexible 2.45-GHz power harvesting wristband with net system output from–24.3 dBm of RF power," *IEEE Trans. Microw. Theory Techn.*, vol. 66, no. 1, pp. 380–395, Jan. 2018.
[26] H. Zhang, Z. Zhong, Y.-X. Guo, and W. Wu, "Differentially-fed charge pumping rectifier design with an enhanced efficiency for ambient RF energy harvesting," in *IEEE MTT-S Int. Microw. Symp. Dig.*, Jun. 2017, pp. 613–616.
[27] C. Song, Y. Huang, J. Zhou, J. Zhang, S. Yuan, and P. Carter, "A high-efficiency broadband rectenna for ambient wireless energy harvesting," *IEEE Trans. Antennas Propag.*, vol. 63, no. 8, pp. 3486–3495, Aug. 2015.
[28] S. D. Assimonis, S.-N. Daskalakis, and A. Bletsas, "Sensitive and efficient RF harvesting supply for batteryless backscatter sensor networks," *IEEE Trans. Microw. Theory Techn.*, vol. 64, no. 4, pp. 1327–1338, Apr. 2016.
[29] M. Mattsson, C. I. Kolitsidas, and B. L. G. Jonsson, "Dual-band dual-polarized full-wave rectenna based on differential field sampling," *IEEE Antennas Wireless Propag. Lett.*, vol. 17, no. 6, pp. 956–959, Jun. 2018.
[30] Z. Zeng, X. Li, A. Bermak, C.-Y. Tsui, and W.-H. Ki, "A WLAN 2.4-GHz RF energy harvesting system with reconfigurable rectifier for wireless sensor network," in *Proc. IEEE Int. Symp. Circuits Syst. (ISCAS)*, Montreal, QC, Canada, May 2016, pp. 2362–2365.
[31] A. Biswas, S. B. Hamidi, C. Biswas, P. Roy, D. Mitra, and D. Dawn, "A novel CMOS RF energy harvester for self-sustainable applications," in *Proc. IEEE 19th Wireless Microw. Technol. Conf. (WAMICON)*, Sand Key, FL, USA, Apr. 2018, pp. 1–5.
[32] M. Taghadosi, L. Albasha, N. A. Quadir, Y. A. Rahama, and N. Qaddoumi, "High efficiency energy harvesters in 65 nm CMOS process for autonomous IoT sensor applications," *IEEE Access*, vol. 6, pp. 2397–2409, Dec. 2018.
[33] M. H. Ouda, M. Arsalan, L. Marnat, A. Shamim, and K. N. Salama, "5.2-GHz RF power harvester in 0.18-μm CMOS for implantable intraocular pressure monitoring," *IEEE Trans. Microw. Theory Techn.*, vol. 61, no. 5, pp. 2177–2184, May 2013.
[34] A. S. Almansouri, M. H. Ouda, and K. N. Salama, "A CMOS RF-to-DC power converter with 86% efficiency and-19.2-dBm sensitivity," *IEEE Trans. Microw. Theory Techn.*, vol. 66, no. 5, pp. 2409–2415, May 2018.
[35] S. Fan, R. Wei, L. Zhao, X. Yang, L. Geng, and P. X.-L. Feng, "An ultralow quiescent current power management system with maximum power point tracking (MPPT) for batteryless wireless sensor applications," *IEEE Trans. Power Electron.*, vol. 33, no. 9, pp. 7326–7337, Sep. 2018.
[36] V. Marian, B. Allard, C. Vollaire, and J. Verdier, "Strategy for microwave energy harvesting from ambient field or a feeding source," *IEEE Trans. Power Electron.*, vol. 27, no. 11, pp. 4481–4491, Nov. 2012.
[37] S. Bandyopadhyay and A. P. Chandrakasan, "Platform architecture for solar, thermal, and vibration energy combining with MPPT and single inductor," *IEEE J. Solid-State Circuits*, vol. 47, no. 9, pp. 2199–2215, Sep. 2012.
[38] S. Fan *et al.*, "A high-efficiency radio frequency rectifier-booster regulator for ambient WLAN energy harvesting applications," in *IEEE MTT-S Int. Microw. Symp. Dig.*, May 2018, pp. 1–3.
[39] S. Dehghani, S. Abbasian, and T. Johnson, "Tracking load to optimize power efficiency in RF to DC rectifier circuits," in *Proc. IEEE Wireless Power Transf. Conf. (WPTC)*, Boulder, CO, USA, May 2015, pp. 1–3.
[40] L. Shen and X. Yang, "A novel rectifier circuit operating at dual-frequencies of 1.8 GHz and 2.4 GHz," in *IEEE MTT-S Int. Microw. Workshop Ser. RF Wireless Technol. Biomed. Healthcare Appl. (IMWS-BIO)*, Singapore, Dec. 2013, pp. 1–3.
[41] B. L. Pham and A.-V. Pham, "Triple bands antenna and high efficiency rectifier design for RF energy harvesting at 900, 1900 and 2400 MHz," in *IEEE MTT-S Int. Microw. Symp. Dig.*, Seattle, WA, USA, Jun. 2013, pp. 1–3.

Shiquan Fan (S'13– M'15) received the B.Sc., M.Sc., and Ph.D. degrees in microelectronics from Xi'an Jiaotong University, Xi'an, China, in 2003, 2009, and 2014, respectively.

From 2003 to 2006, he was a Research and Development Engineer for power management system design and development. From 2016 to 2017, he was a Visiting Scholar with the Department of Electrical Engineering and Computer Science, Case Western Reserve University, Cleveland, OH, USA. He is currently an Associate Professor with the School of Microelectronics, Xi'an Jiaotong University. His current research interests include analog and mixed-signal integrated circuit, energy harvesting system, power management circuit, and system design.

Dr. Fan was a recipient of the Science and Technology Improvement Award by Shaanxi Municipal Government in 2015 and the Lam Research Thesis Award twice from Lam Research Corporation in 2015.

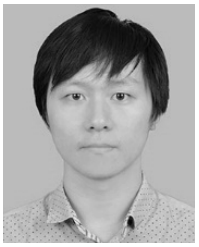

Zheyi Yuan received the B.Sc. degree in microelectronics from Xi'an Jiaotong University, Xi'an, China, in 2017, where he is currently pursuing the M.S. degree in microelectronics.

His current research interests include RF energy harvesting and power management circuits.

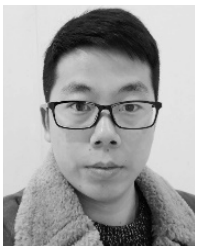

Wei Gou (S'18) received the B.Sc. and M.S. degrees in microelectronics from Xi'an Jiaotong University, Xi'an, China, in 2015 and 2018, respectively.

In 2018, he joined Huawei Technologies Co., Ltd., Xi'an, as an Analog IC Design Engineer. His current research interests include power management circuits and systems and all-digital phase lock loops.

Yang Zhao received the B.Sc. degree in microelectronics from Xi'an Jiaotong University, Xi'an, China, in 2016, where he is currently pursuing the M.S. degree in microelectronics.

His current research interests include piezoelectric energy harvesting and power management circuits.

Chaoyun Song (M'16) received the B.Sc., M.Sc., and Ph.D. degrees in electrical engineering and electronics from the University of Liverpool (UoL), Liverpool, U.K., in 2012, 2013, and 2017, respectively.

From 2015 to 2016, he was a Research Assistant and an Antenna Design Engineer with UoL and BAE Systems, Chelmsford, U.K. He is currently a Post-Doctoral Research Associate with UoL. He has authored or coauthored more than 30 papers in internationally refereed journals and conference proceedings. He has filed six U.S., EU, and U.K. patents. His current research interests include liquid antennas, novel materials, wireless energy harvesting, rectifying antennas, wireless power transfer, global navigation satellite system antennas, anti-jamming technologies, and smart sensors for the Internet of Things.

Dr. Song was a recipient of many international awards, such as the recipient of the IET Present Around the World Competition in 2016, the EW BrightSparks Award for Outstanding Electronic Engineers under age 30 in the U.K., 2018, and the BAE Systems Chairman's Award in 2017 for the innovation of next generation global navigation satellite system antennas. He has been a regular Reviewer of many international journals, including *Applied Physics Letters*, *Scientific Reports*, the IEEE TRANSACTIONS ON ANTENNAS AND PROPAGATION, the IEEE TRANSACTIONS ON INDUSTRIAL ELECTRONICS, the IEEE TRANSACTIONS ON MICROWAVE THEORY AND TECHNIQUES, the IEEE TRANSACTION ON CIRCUITS AND SYSTEMS—I: REGULAR PAPERS, the IEEE ANTENNAS AND WIRELESS PROPAGATION LETTERS, and IEEE SENSORS LETTERS.

Yi Huang (S'91–M'96–SM'06) received the B.Sc. degree in physics from Wuhan University, Wuhan, China, in 1984, the M.Sc. (Eng.) degree in microwave engineering from the Nanjing Research Institute of Electronics Technology (NRIET), Nanjing, China, in 1987, and the D.Phil. degree in communications from the University of Oxford, Oxford, U.K., in 1994.

Since 1987, he has been conducting research on wireless communications, applied electromagnetics, radar, and antennas. His experience includes three years spent with NRIET as a Radar Engineer and various periods with the Universities of Birmingham, Oxford and Essex, U.K., as a Member of Research Staff. In 1994, he joined British Telecom Labs, as a Research Fellow. In 1995, he joined the Department of Electrical Engineering and Electronics, University of Liverpool, Liverpool, U.K., where he is currently a Full Professor of wireless engineering, the Head of the High Frequency Engineering Group, and the Deputy Head of the Department. He has been a Consultant to various companies. He has authored or coauthored more than 350 refereed papers in leading international journals and conference proceedings. He authored *Antennas: from Theory to Practice* (Wiley, 2008) and *Reverberation Chambers: Theory and Applications to EMC and Antenna Measurements* (Wiley, 2016).

Mr. Huang is a Fellow of the IET and a Senior Fellow of the HEA. He was a recipient of many research grants from research councils, government agencies, charity, EU and industry, and served on a number of national and international technical committees. He has been an Editor, Associate Editor, or a Guest Editor of five international journals. He has been a Keynote/Invited Speaker and an organizer of many conferences and workshops (e.g., WiCom 2006, 2010, IEEE iWAT2010, LAPC2012, and EuCAP2018). He is currently the Editor-in-Chief of *Wireless Engineering and Technology* and an Associate Editor of the IEEE ANTENNAS AND WIRELESS PROPAGATION LETTERS, and the Ireland Representative to the European Association of Antenna and Propagation (EurAAP).

Jiafeng Zhou received the Ph.D. degree in electrical engineering and electronics from the University of Birmingham, Birmingham, U.K., in 2004.

He then moved to the Department of Electronic and Electrical Engineering, University of Bristol, Bristol, U.K., until 2013, where he was involved in the development of highly efficient and linear amplifiers. In 1997, he was with the National Meteorological Satellite Centre of China, Beijing, China, where he was involved in the development of communication systems for Chinese geostationary meteorological satellites. From 2004 to 2006, he was a Research Fellow with the University of Birmingham, where he was involved in phased arrays for reflector observing systems. He is currently with the Department of Electrical Engineering and Electronics, University of Liverpool, Liverpool, U.K. His current research interests include microwave power amplifiers, filters, electromagnetic energy harvesting, and wireless power transfer.

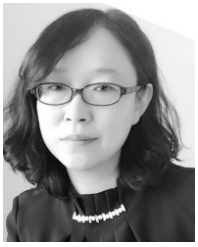

Li Geng (M'06) received the B.Sc. degree in physics, and the M.Sc. and Ph.D. degrees in electrical engineering from the Xi'an University of Technology, Xi'an, China, in 1990, 1998, and 2001, respectively.

She was the Director of the Department of Microelectronics, Xi'an Jiaotong University, Xi'an. From 1999 to 2000, she was a Visiting Scholar with the Department of Electrical Engineering, Ilmenau University of Technology, Ilmenau, Germany. From 2007 to 2008, she was a Visiting Professor with the Department of Electrical Engineering, Stanford University, Stanford, CA, USA. She is currently a Professor with the Department of Microelectronics, Xi'an Jiaotong University. Her current research interests include power management integrated circuits, low-voltage low-power analog and mixed-signal integrated circuits, RF integrated circuit, and bioimplant systems.

Dr. Geng was a Technical Program Committee member of ASSCC from 2010 to 2018. She was a recipient of the Science and Technology Improvement Award of the Ministry of National Mechanical Industry, China, in 1999 and the Science and Technology Improvement Award by Shaanxi Municipal Government in 2000, 2001, 2010, and 2015, respectively.